Hindawi Publishing Corporation
International Journal of Photoenergy
Volume 2014, Article ID 153428, 7 pages
http://dx.doi.org/10.1155/2014/153428

Research Article

A Simple and Efficient MPPT Method for Low-Power PV Cells

Maria Teresa Penella[1] and Manel Gasulla[2]

[1] *Urbiotica S.L, Parc UPC, Edifici Nexus II, C/Jordi Girona 29, 08034 Barcelona, Spain*
[2] *Universitat Politècnica de Catalunya, C/Esteve Terradas 7, 08860 Castelldefels, Spain*

Correspondence should be addressed to Manel Gasulla; manel.gasulla@upc.edu

Received 31 October 2013; Accepted 28 December 2013; Published 27 February 2014

Academic Editor: Ismail H. Altas

Small-size PV cells have been used to power sensor nodes. These devices present limited computing resources and so low complexity methods have been used in order to extract the maximum power from the PV cells. Among them, the fractional open circuit voltage (FOCV) method has been widely proposed, where the maximum power point of the PV cell is estimated from a fraction of its open circuit voltage. Here, we show a generalization of the FOCV method that keeps its inherent simplicity and improves the tracking efficiency. First, a single-diode model for PV cells was used to compute the tracking efficiency versus irradiance. Computations were carried out for different values of the parameters involved in the PV cell model. The proposed approach clearly outperformed the FOCV method, specially at low irradiance, which is significant for powering sensor nodes. Experimental tests performed with a 500 mW PV panel agreed with these results.

1. Introduction

The advances in electronics and communication protocols have led to a widespread use of wireless sensor networks (WSN). In most applications, the sensor nodes of the WSN are required to be wireless both for communication and powering. As for the power supply, the use of small-size PV cells or modules has been proposed. The power-voltage (P-V) curve of a photovoltaic (PV) cell or panel presents a maximum power point (MPP) that changes with temperature and irradiance. To extract the maximum power under varying conditions an MPP tracker can be used. Several MPP tracking (MPPT) methods have been proposed in the literature [1–4]. Since sensor nodes present limited computing resources, low complexity MPPT methods are preferred for this particular application. Because the location of the sensor nodes is mostly determined by the application, a wide range of irradiance can be expected at the sensor placement. Thus, a high efficiency is desirable over a wide range of irradiance, and specially for low irradiance as the power source is scarce.

One of the simplest and most popular MPPT methods is the fractional open circuit voltage (FOCV) technique, which estimates the MPP voltage (V_{MPP}) from a fraction of the open circuit voltage (V_{OC}); that is,

$$V_{MPP,est} = kV_{OC}, \quad (1)$$

where $V_{MPP,est}$ is the estimated value of the actual V_{MPP} and k is an empirical constant whose value should be set following a thorough characterization of the PV panel under varying meteorological conditions (irradiance and cell temperature). V_{OC} is either measured periodically (by momentarily opening the output of the PV panel) or by using a pilot cell (i.e., an additional solar cell of the same type configured in open circuit voltage configuration). Typical reported values for k range from 0.73 to 0.8 depending on the PV panel type and characteristics [2, 3]. Because of its simplicity, the FOCV method has been recently applied to small-size PV cells in order to power autonomous sensors [5–9].

In this work, we propose to generalize (1) in order to estimate V_{MPP} by using a linear fit; that is,

$$V_{MPP,est} = aV_{OC} + b, \quad (2)$$

where a and b are empirical coefficients. The use of (2) will be referred to as the linear open circuit voltage (LOCV)

method. In fact, the FOCV method can be considered a particular case of the proposed LOCV method with $b = 0$. Both computed and experimental results of the proposed approach will be presented and compared with the FOCV method. As will be shown, the LOCV method significantly improves the performance of the FOCV method, especially at low irradiance, while maintaining its inherent simplicity. The work presented here builds upon [10], where we first presented (2) and some initial results.

2. Solar Cell Model

Different equivalent circuits have been used in the literature in order to model the current/voltage (I-V) characteristic of a silicon PV cell [11–15]. Among them, the single-diode model, shown in Figure 1, offers a good compromise between simplicity and accuracy [13], whereby I_{PH} is the photogenerated current, I is the cell current, V is the cell voltage, and R_s and R_p are, respectively, the series and shunt resistances. This model will be used here in order to generate computed data of the I-V curve of a PV cell.

The corresponding expression of the I-V characteristic is given by [16]

$$I = I_{SC} - I_O \left[e^{((q(V+R_sI))/n_dKT_{cell})} - 1\right] - \frac{V + R_sI}{R_p}, \quad (3)$$

where I_{PH} has been approximated by I_{SC}, the short circuit current of the cell; I_O is the saturation current of the diode; q is the electron charge; n_d is the ideality factor of the diode, which, for silicon, is usually between 1 and 2 [5, 7]; K is the Boltzmann constant; and T_{cell} is the cell temperature in Kelvin.

By considering open circuit conditions ($I = 0$ and $V = V_{OC}$) in (3), we can write the parameter I_O as

$$I_O = \frac{I_{SC} - \left(V_{OC}/R_p\right)}{\left[e^{(qV_{OC}/n_dKT_{cell})} - 1\right]}. \quad (4)$$

The parameters I_{SC} and V_{OC} in (3) and (4) change with the irradiance and temperature as

$$I_{SC}\left(T_{cell}, G\right) = \frac{G}{1000}\left[I_{SC_r} + \alpha\left(T_{cell} - T_r\right)\right], \quad (5)$$

$$V_{OC}\left(T_{cell}, G\right) = \left[V_{OC_r} + \beta\left(T_{cell} - T_r\right)\right] \times \left[1 + \rho_{OC}\ln\left(\frac{G}{G_{OC}}\right)\ln\left(\frac{G}{G_r}\right)\right], \quad (6)$$

where T_{cell} is the cell temperature; G is the incident irradiance (in W/m^2); α and β are the current and voltage temperature coefficients, respectively; I_{SC_r} and V_{OC_r} are given at a reference irradiance (G_r) and reference cell temperature (T_r); and ρ_{OC} and G_{OC} are two empirical constants used to model the significant variation of V_{OC} at low G. Typically, $G_r = 1000$ W/m^2 (=100 mW/cm^2) and $T_r = 25^\circ$C. Values of $\rho_{OC} = -0.04$ and $G_{OC} = 1000$ W/m^2 are adequate for many silicon PV cells [17]. When directly illuminated, solar cells heat up above the ambient temperature (T_a), which is known as the self-heating effect, and T_{cell} can be obtained from

$$T_{cell} = T_a + \frac{T_{cell,NOCT} - 20}{800\ \text{W/m}^2}G. \quad (7)$$

where $T_{cell,NOCT}$, known as the *nominal operating cell temperature* (NOCT), is the temperature of the cell when exposed to 800 W/m^2 at $T_a = 20^\circ$C and wind speed of 1 m/s. It is empirically determined, and for silicon solar cells range between 42°C and 48°C.

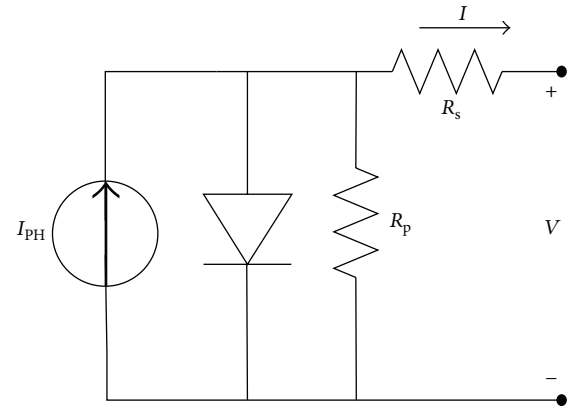

Figure 1: Single-diode model of a solar cell with series (R_s) and shunt (R_p) resistances.

3. Computed Results

We employed (3) to (7) with the following parameter values typical of monocrystalline solar cells [17]: $J_{SC_r} = 35$ mA/cm^2; $V_{OC_r} = 0.6$ V; $\alpha/A = 12.5\,\mu$A/cm^2/°C; $\beta = -2$ mV/°C; and $T_{cell,NOCT} = 42^\circ$C. The parameters I_{SC_r} and α in (5) can be, respectively, obtained by multiplying J_{SC_r} and α/A by the area of the cell. For the computations, a single solar cell with an area of 1 cm^2 was used. Nevertheless, as will be justified at the end of this section, the results and the derived conclusions are equally valid to cells of any area and PV panels composed of an arbitrary number of solar cells disposed in parallel and series. Figure 2 shows the computed I-V and P-V curves at three different levels of irradiance for the particular case of $R_s = 0$, $R_p = \infty$, $n_d = 1.5$, and $T_a = 25^\circ$C. To obtain the data we simulated the PV cell model in SPICE. The power values were obtained by multiplying I by V at each data point. As can be seen, both V_{OC} and V_{MPP} slightly decrease at the highest irradiance, which is due to the self-heating effect of the PV cell.

From the data of the I-V and P-V curves, several parameters can be obtained such as V_{OC}, V_{MPP}, and P_{MPP} (power at the MPP). Table 1 shows numerical values of those parameters for an irradiance range from *ca.* 20 W/m^2 to 1000 W/m^2. Fourteen points of irradiance, logarithmically equally spaced, were selected to provide a dynamic range around 100 in P_{MPP}. Other cases that will be discussed throughout this section are also shown in Table 1. Figure 3

Table 1: Computed V_{OC}, V_{MPP}; and P_{MPP} data at fourteen points of irradiance, logarithmically equally spaced, and for different values of the parameters of the PV cell model.

G	n_d = 1.5 (Figure 1)			n_d = 1			n_d = 2			r_s = 0.1 (Figure 6)			r_p = 10 (Figure 8)		
(W/m^2)	V_{OC} (V)	V_{MPP} (V)	P_{MPP} (mW)	V_{OC} (V)	V_{MPP} (V)	P_{MPP} (mW)	V_{OC} (V)	V_{MPP} (V)	P_{MPP} (mW)	V_{OC} (V)	V_{MPP} (V)	P_{MPP} (mW)	V_{OC} (V)	V_{MPP} (V)	P_{MPP} (mW)
23.7	0.262	0.194	0.135	0.262	0.207	0.153	0.262	0.185	0.121	0.262	0.193	0.134			
31.6	0.311	0.237	0.227	0.311	0.251	0.254	0.311	0.226	0.205	0.311	0.235	0.225			
42.2	0.357	0.277	0.362	0.357	0.293	0.401	0.357	0.264	0.330	0.357	0.275	0.359	0.241	0.126	0.095
56.2	0.398	0.313	0.553	0.398	0.331	0.609	0.398	0.300	0.507	0.398	0.311	0.548	0.306	0.168	0.168
75	0.434	0.347	0.826	0.434	0.365	0.904	0.434	0.332	0.761	0.434	0.343	0.816	0.369	0.221	0.299
100	0.467	0.376	1.2	0.467	0.396	1.312	0.467	0.361	1.113	0.467	0.372	1.186	0.42	0.282	0.524
133.4	0.495	0.402	1.725	0.495	0.422	1.874	0.495	0.385	1.600	0.495	0.395	1.693	0.462	0.337	0.899
177.8	0.518	0.423	2.431	0.518	0.444	2.635	0.518	0.406	2.259	0.518	0.415	2.374	0.494	0.379	1.477
237.1	0.537	0.440	3.38	0.537	0.461	3.657	0.537	0.422	3.146	0.537	0.429	3.279	0.519	0.409	2.321
316.2	0.55	0.452	4.64	0.55	0.474	5.013	0.55	0.434	4.321	0.55	0.437	4.458	0.537	0.43	3.500
421.7	0.558	0.458	6.28	0.558	0.481	6.786	0.558	0.441	5.853	0.558	0.439	5.961	0.548	0.443	5.094
562.3	0.56	0.459	8.386	0.56	0.482	9.067	0.56	0.441	7.812	0.56	0.433	7.821	0.553	0.448	7.185
749.9	0.555	0.454	11.031	0.555	0.477	11.943	0.555	0.436	10.264	0.555	0.42	10.035	0.55	0.446	9.850
1000	0.543	0.442	14.254	0.543	0.464	15.472	0.543	0.424	13.234	0.543	0.398	12.511	0.54	0.436	13.13

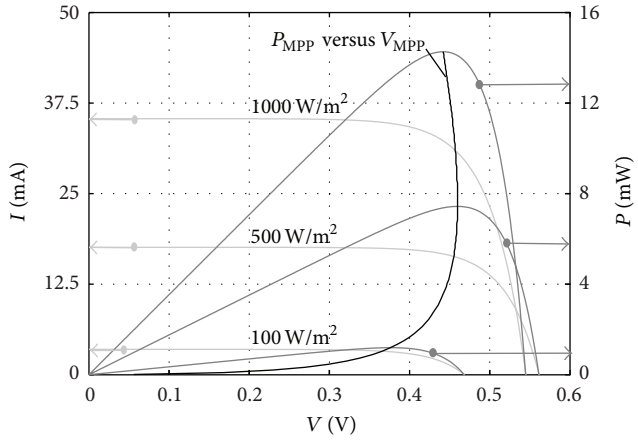

Figure 2: Generic I-V and P-V plots at several values of G and at T_a = 25°C for a single solar cell with an area of 1 cm^2. A curve joining the MPPs is also plotted.

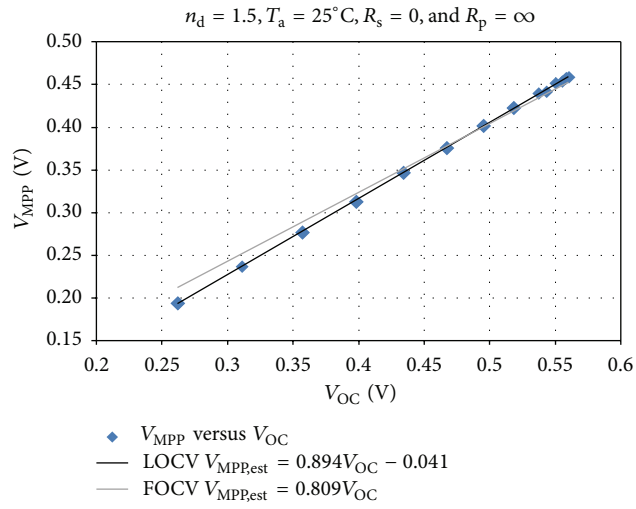

Figure 3: Computed V_{MPP} versus V_{OC} for a single PV cell. Two least-square regression lines are also represented: the grey line corresponds to the FOCV method with k = 0.809 whereas the black line corresponds to the LOCV method with a = 0.894 and b = −0.041. The parameters of the PV cell model are T_a = 25°C, n_d = 1.5, R_s = 0, and R_p = ∞.

represents the fourteen computed points (diamonds) of V_{MPP} versus V_{OC} and two least-squares regression lines fitted to the computed data corresponding, respectively, to the FOCV method, that is, (1) with k = 0.809, and the LOCV method, that is, (2) with a = 0.894 and b = −0.041. As can be seen, the regression line corresponding to the LOCV method better fits the computed data. The inferred parameters of the regression lines (k, a, and b) were used to obtain $V_{MPP,est}$ at the fourteen irradiance points for each of the two methods, by using (1) and (2), respectively.

The corresponding power values at $V_{MPP,est}$, $P_{MPP,est}$ were inferred from the computed P-V curves in order to obtain the tracking efficiency, which is given by

$$\eta_{MPP} = \frac{P_{MPP,est}}{P_{MPP}}. \quad (8)$$

This parameter is used in the literature to compare the performance among different algorithms. Obviously, a value of 1 (100%) is the ultimate goal. Figure 4 shows the computed values of η_{MPPT} versus G at T_a = 25°C for the fourteen irradiance points. We added the results at two more temperatures, 0°C and 50°C. For these temperatures, the P-V curves were recalculated but we still used the same regression lines of Figure 3. This makes sense, as a PV panel can be characterized at a single temperature, for example, 25°C, and the calculated regression lines used for

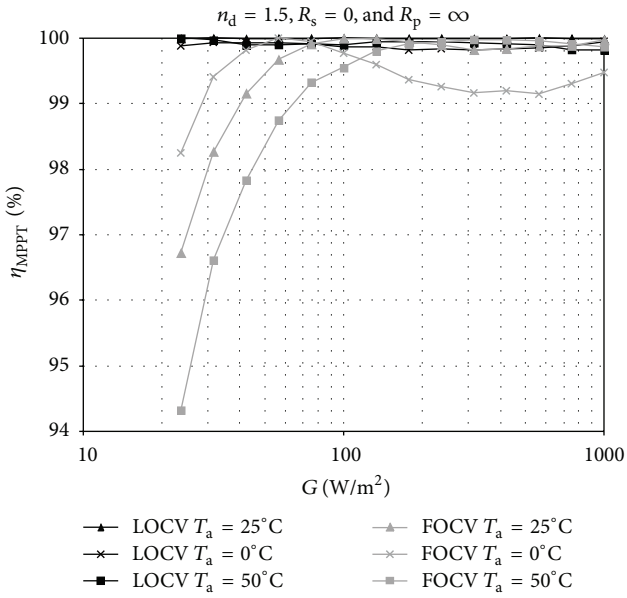

FIGURE 4: Computed η_{MPPT} versus G by using the FOCV and LOCV methods for a single PV cell at different values of T_a and with $n_d = 1.5$, $R_s = 0$, and $R_p = \infty$.

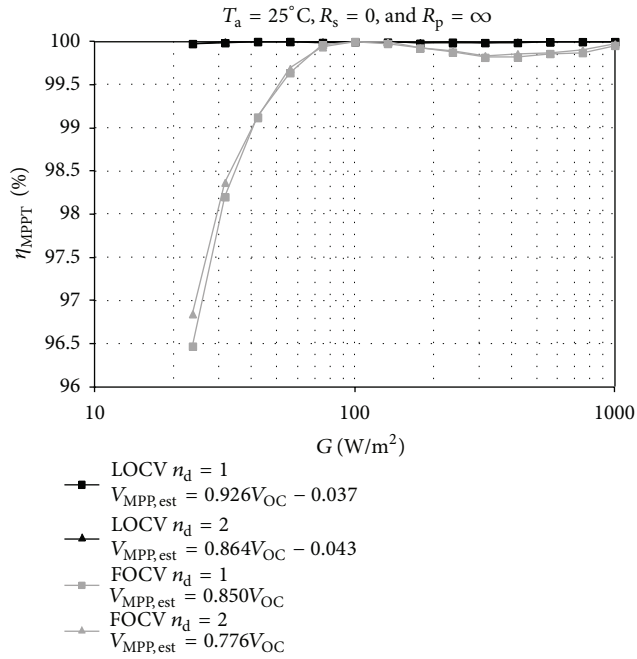

FIGURE 5: Computed η_{MPPT} versus G by using the FOCV and LOCV methods for a single PV cell at different values of n_d and with $T_a = 25^\circ$C, $R_s = 0$, and $R_p = \infty$.

the full working temperature range. As can be seen, at low irradiance the LOCV method clearly outperforms the FOCV method. At higher irradiance, a rather high value of η_{MPPT} (>99%) is achieved by both methods, although the FOCV method presents the lowest efficiency from *ca*. 100 W/m^2 to 1000 W/m^2 at $T_a = 0^\circ$C. The value of η_{MPPT} for the LOCV method was always higher than 99.8% at the three computed temperatures.

More computations were carried out at $T_a = 25^\circ$C for $n_d = 1$ and $n_d = 2$ (see Table 1). Again, better linear fits were obtained with the LOCV method (not shown). Figure 5 shows the corresponding computed values of η_{MPPT}. For each of the cases, the parameters of the corresponding regression lines are provided. Again, the LOCV method clearly outperforms the FOCV method at low irradiance and slightly at medium irradiance.

Finally, computations were performed for $n_d = 1.5$, $T_a = 25^\circ$C, nonzero values of R_s, and finite values of R_p. In [13] normalized values for R_s and R_p were defined as

$$r_s = \frac{R_s}{[V_{OC}/I_{SC}]_{STC}}, \qquad r_p = \frac{R_p}{[V_{OC}/I_{SC}]_{STC}}. \tag{9}$$

This normalization allows for an immediate comparison among different PV modules (of different area and characteristics). Based on [13], in our work we considered the following values: from 0.01 to 0.1 for r_s and from 100 to 10 for r_p. The performance for both $r_s = 0.01$ and $r_p = 100$ was almost identical to that shown in Figure 2 (for $T_a = 25^\circ$C), with the LOCV method outperforming the FOCV method. So these results are not shown here. Table 1 shows the data for the limiting cases $r_s = 0.1$ (with $r_p = \infty$) and $r_p = 10$ (with $r_s = 0$). For the case of $r_p = 10$, the data for the lowest two irradiance levels were not used as they provided negligible values of P_{MPP} (well below of 1% of the resulting P_{MPP} at 1000 W/m^2). As for $r_s = 0.1$, Figure 6 shows the computed values of V_{MPP} versus V_{OC} and the fitted regression lines. Due to the high value of r_s (highest limit), the data values present a folded form at the highest irradiance levels. So the regression lines of the FOCV and LOCV methods cannot fit the data corresponding to the high irradiance levels as well as that in Figure 3. Otherwise, both lines are very similar in this case. Consequently, the computed values of η_{MPPT}, shown in Figure 7 ($r_s = 0.1$), are quite similar (and indeed relatively high) for both methods.

As for $r_p = 10$, Figure 8 again shows the computed values of V_{MPP} versus V_{OC} and the fitted regression lines. Due to the low relative value of r_p (lowest limit) the regression line of the LOCV method cannot fit the data corresponding to the low irradiance levels as well as that in Figure 3. Even so, the computed values of η_{MPPT}, also shown in Figure 7, still present a high efficiency, outperforming the FOCV method at all the irradiance levels, but specially at the low ones. Finally, we computed η_{MPPT} for $r_s = 0.1$ and $r_p = 10$ (not shown). In that case, the LOCV method also outperformed the FOCV method at low and medium irradiance levels.

Increasing the PV cell area or adding identical PV cells in parallel will scale up the values of currents and thus of powers but the values of V_{OC} and V_{MPP} will remain the same and so the derived tracking efficiencies. Tracking efficency will also

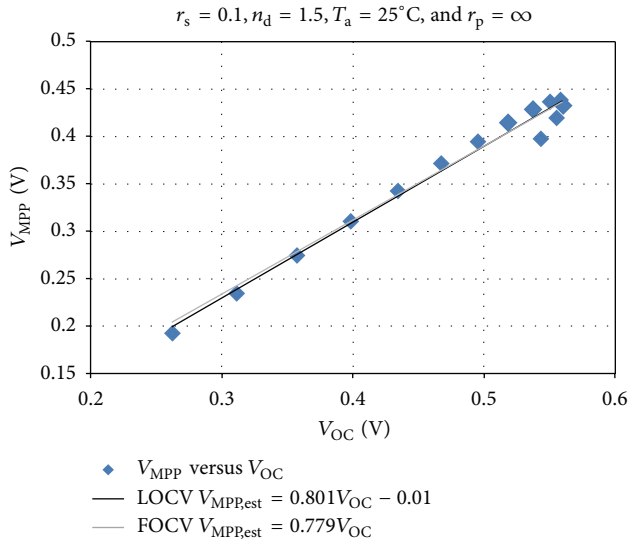

FIGURE 6: Computed V_{MPP} versus V_{OC} for a single PV cell with $T_a = 25^\circ C$, $n_d = 1.5$, $r_p = \infty$, and $r_s = 0.1$. Two regression lines corresponding to the FOCV and LOCV methods are also represented.

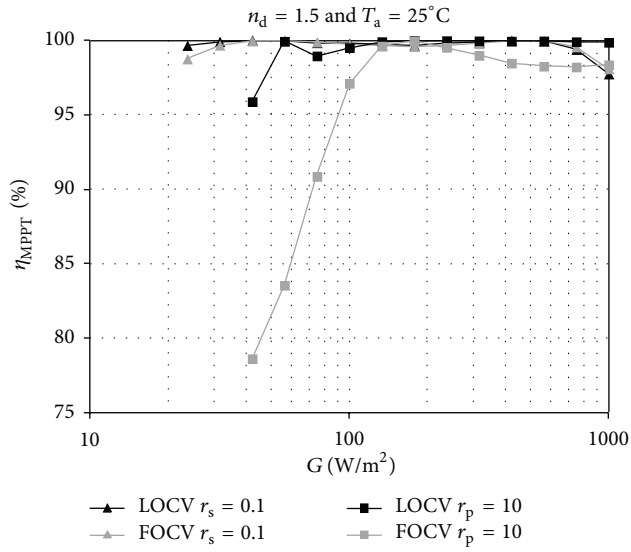

FIGURE 7: Computed η_{MPPT} versus G by using the FOCV and the LOCV methods for a single PV cell with $T_a = 25^\circ C$, $n_d = 1.5$, and for both $r_s = 0.1$ (and $r_p = \infty$) and $r_p = 10$ (and $r_s = 0$).

remain constant by adding PV cells in series: both V_{MPP} and V_{OC} will scale up by the number of serial cells but their ratio will remain constant and so the derived tracking efficiencies.

4. Experimental Results

The LOCV method was tested with a 500 mW ($I_{SC} = 160$ mA, $V_{OC} = 4.6$ V) PV panel (MSX-005, Solarex) and compared with the FOCV method. These low-power panels are used, for example, to power autonomous sensors [5–10]. In order

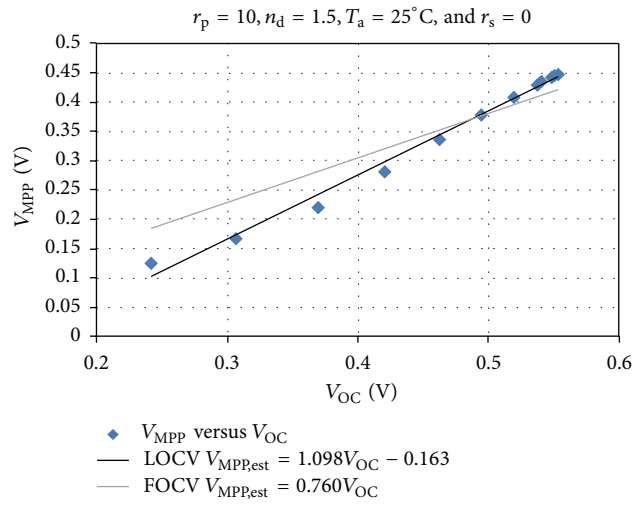

FIGURE 8: Computed V_{MPP} versus V_{OC} for a single PV cell with $T_a = 25^\circ C$, $n_d = 1.5$, $r_s = 0$, and $r_p = 10$. Two regression lines corresponding to the FOCV and LOCV methods are also represented.

to achieve reproducible results, we implemented a PV panel simulator by connecting a current source (GS610, Yokogawa) in parallel with the PV panel, which was coated with an opaque cover (Figure 9). In this way, the short circuit current (I_{SC}) of the PV panel was adjusted by the current source, emulating different levels of irradiance. Since the panel was not illuminated, $T_{celL,NOCT} = 20^\circ C$ (i.e., the panel is not overheated). The current source was configured to cover the full range of the PV panel, varying from 5 mA to 158 mA in 9 mA steps. The PV panel simulator was characterized by using the GS610's measurement unit to measure the panel's voltage, a 2001 multimeter (Keithley) to measure the current of the panel, and a programmable voltage source (Agilent E3631A) in parallel with a 10 Ω/1 W resistor acting as a load. Figure 9 shows the experimental setup.

All the instruments were controlled via the GPIB bus with a dedicated program using the graphical development environment LabVIEW. For each current value (I_{SC}), the voltage of the E3631A was increased from 0 V to 5 V in 0.1 V steps. PV output voltages and currents were measured and the corresponding power values were calculated in order to obtain the *I-V* and *P-V* curves. From each *P-V* curve the values of V_{OC}, V_{MPP}, and P_{MPP} were obtained. The limit values for P_{MPP} were, respectively, 8.2 mW ($I_{SC} = 5$ mA) and 545.9 mW ($I_{SC} = 158$ mA).

Figure 10 represents the experimental data of V_{MPP} versus V_{OC} and two fitted least-squares regression lines corresponding to the FOCV and LOCV methods. As can be seen, the regression line corresponding to the LOCV method better fits the experimental data. From the two regression lines, the values of $V_{MPP,est}$ corresponding to the FOCV and LOCV methods were derived. Then, from the *P-V* curves, the values of $P_{MPP,est}$ and η_{MPPT} were obtained. Figure 11 shows η_{MPPT} versus P_{MPP}. In agreement with the computed results of Section 3, the LOCV method clearly outperformed the

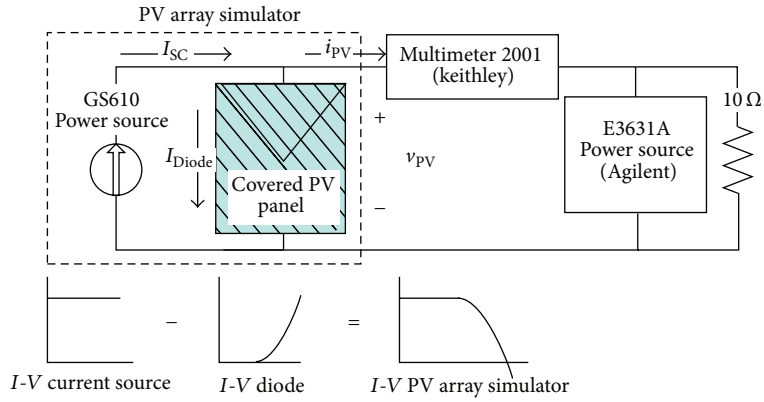

Figure 9: The PV array simulator and the setup used for its characterization.

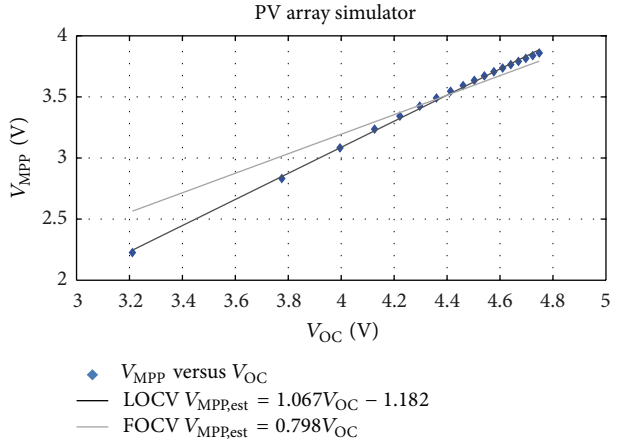

Figure 10: V_{MPP} versus V_{OC} for a 500 mW panel simulator at T_a = 25°C and two fitted least-square regression lines corresponding to the FOCV and LOCV methods.

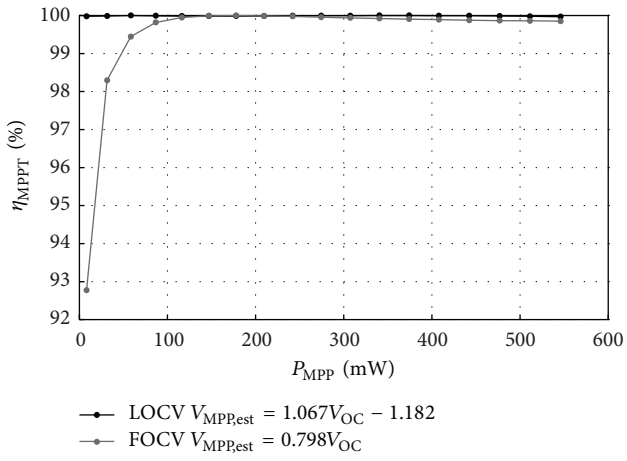

Figure 11: Experimental η_{MPPT} versus P_{MPP} by using the FOCV method (grey line), with k = 0.798, and the LOCV method (black line), with a = 1.0674 and b = −1.182, for a 500 mW PV panel.

FOCV method at low irradiance, with η_{MPPT} always being higher than 99.96%. The efficiency increase at low irradiance is of significant importance in order to power sensor nodes.

5. Conclusion

PV cells have been proposed in the literature in order to power the sensor nodes of WSN. Because of the limited computing capabilities of the sensor nodes, simple MPPT methods have to be used. Among them, the FOCV method has been widely proposed and used. Tracking efficiencies, though, are lower than that achieved with more complex methods. In this work, we have proposed the LOCV method, which outperforms the FOCV method while maintaining its inherent simplicity. Computations show that the LOCV method achieves a high efficiency for all the irradiance range whereas the FOCV method fails in achieving a high efficiency at low irradiance levels for most of the cases. The presence of extremely low values of shunt resistance of the PV cell negatively impacts the achieved efficiency on both methods but specially that of the FOCV method. Finally, experimental data from a low-power 500 mW PV panel confirmed the good performance of the LOCV method for a wide range of irradiance, which is of significant value for powering sensor nodes.

Conflict of Interests

The authors declare that there is no conflict of interests regarding the publication of this paper.

Acknowledgment

This work was supported by the Spanish Ministry of Economy and Competitiveness under Contract TEC2011-27397.

References

[1] T. Esram and P. L. Chapman, "Comparison of photovoltaic array maximum power point tracking techniques," *IEEE Transactions on Energy Conversion*, vol. 22, no. 2, pp. 439–449, 2007.

[2] N. Onat, "Recent developments in maximum power point tracking technologies for photovoltaic systems," *International Journal of Photoenergy*, vol. 2010, Article ID 245316, 11 pages, 2010.

[3] D. P. Hohm and M. E. Ropp, "Comparative study of maximum power point tracking algorithms," *Progress in Photovoltaics: Research and Applications*, vol. 11, no. 1, pp. 47–62, 2003.

[4] V. Salas, E. Olías, A. Barrado, and A. Lázaro, "Review of the maximum power point tracking algorithms for stand-alone photovoltaic systems," *Solar Energy Materials and Solar Cells*, vol. 90, no. 11, pp. 1555–1578, 2006.

[5] D. Dondi, A. Bertacchini, D. Brunelli, L. Larcher, and L. Benini, "Modeling and optimization of a solar energy harvester system for self-powered wireless sensor networks," *IEEE Transactions on Industrial Electronics*, vol. 55, no. 7, pp. 2759–2766, 2008.

[6] A. S. Weddell, G. V. Merrett, and B. M. Al-Hashimi, "Photovoltaic sample-and-hold circuit enabling MPPT indoors for low-power systems," *IEEE Transactions on Circuits and Systems I*, vol. 59, no. 6, pp. 1196–1204, 2012.

[7] A. Chini and F. Soci, "Boost-converter-based solar harvester for low power applications," *Electronics Letters*, vol. 46, no. 4, pp. 296–298, 2010.

[8] F. I. Simjee and P. H. Chou, "Efficient charging of supercapacitors for extended lifetime of wireless sensor nodes," *IEEE Transactions on Power Electronics*, vol. 23, no. 3, pp. 1526–1536, 2008.

[9] O. Lopez-Lapeña and M. T. Penella, "Low-power FOCV MPPT controller with automatic adjustment of the sample&hold," *Electronics Letters*, vol. 48, no. 20, pp. 1301–1303, 2012.

[10] M. T. Penella and M. Gasulla, "Optical energy harvesting," in *Powering Autonomous Sensors*, chapter 5, section 5.5, pp. 101–107, Springer, Dordrecht, The Netherlands, 2011.

[11] J. A. Gow and C. D. Manning, "Development of a photovoltaic array model for use in power-electronics simulation studies," *IEE Proceedings: Electric Power Applications*, vol. 146, no. 2, pp. 193–200, 1999.

[12] M. G. Villalva, J. R. Gazoli, and E. R. Filho, "Comprehensive approach to modeling and simulation of photovoltaic arrays," *IEEE Transactions on Power Electronics*, vol. 24, no. 5, pp. 1198–1208, 2009.

[13] C. Carrero, J. Amador, and S. Arnaltes, "A single procedure for helping PV designers to select silicon PV modules and evaluate the loss resistances," *Renewable Energy*, vol. 32, no. 15, pp. 2579–2589, 2007.

[14] W. de Soto, S. A. Klein, and W. A. Beckman, "Improvement and validation of a model for photovoltaic array performance," *Solar Energy*, vol. 80, no. 1, pp. 78–88, 2006.

[15] F. Adamo, F. Attivissimo, A. Di Nisio, and M. Spadavecchia, "Characterization and testing of a tool for photovoltaic panel modeling," *IEEE Transactions on Instrumentation and Measurement*, vol. 60, no. 5, pp. 1613–1622, 2011.

[16] F. Lasnier and T. G. Ang, *Photovoltaic Engineering Handbook*, Adam Hilger, New York, NY, USA, 1990.

[17] A. Luque and S. Hegedus, *Handbook of Photovoltaic Science and Engineering*, 2003.